Biomaterials Science

ROYAL SOCIETY OF CHEMISTRY

PAPER

View Article Online
View Journal | View Issue



Cite this: *Biomater. Sci.*, 2022, **10**, 7042

# Stepwise photothermal therapy and chemotherapy by composite scaffolds of gold nanoparticles, BP nanosheets and gelatin immobilized with doxorubicin-loaded thermosensitive liposomes†

Huajian Chen, [a,b] Rui Sun,[a,b] Tianjiao Zeng,[a,b] Jing Zheng, [a,b] Toru Yoshitomi, [a] Naoki Kawazoe,[a] Yingnan Yang[c] and Guoping Chen *[a,b]

In recent years, the synergistic effect of photothermal therapy (PTT) and chemotherapy has been recognized as an effective strategy for cancer treatment. Controlling the PTT temperature and drug release profile is desirable for minimizing the unexpected damage to normal cells. In this study, a smart platform of stepwise PTT and chemotherapy has been developed by using composite porous scaffolds of biodegradable black phosphorus (BP) nanosheets, gold nanorods(AuNRs), doxorubicin (Dox)-encapsulated thermosensitive liposomes and biodegradable polymers. Under near-infrared (NIR) laser irradiation, the composite scaffolds could attain high and low local temperatures before and after BP degradation, respectively. Dox release from the composite scaffolds could be controlled by the temperature change. *In vitro* cell culture and *in vivo* animal experiments indicated that a strong synergistic effect of PTT and chemotherapy could be achieved at an early stage of treatment before BP degradation, and a mild hyperthermia effect was shown for chemotherapy in the late stage after BP degradation. Moreover, the composite scaffolds after the complete release of Dox could support the proliferation of mesenchymal stem cells. The composite scaffolds showed a synergistic effect of stepwise PTT and chemotherapy for breast cancer elimination and promoted stem cell activities after killing cancer cells.

Received 22nd July 2022,
Accepted 17th October 2022

DOI: 10.1039/d2bm01155g

rsc.li/biomaterials-science



## Introduction

A combination of different cancer therapeutic methods has been developed as an attractive strategy for cancer therapy to achieve a synergistic effect of different therapies.[1,2] PTT and chemotherapy have been used together to maximize their therapeutic effects.[3,4] PTT ablates cancer cells by creating a localized hyperthermia environment with the help of photothermal agents and near-infrared (NIR) lasers.[5–7] Chemotherapy uses anticancer drugs to kill cancer cells.[8] To effectively combine PTT and chemotherapy, thermosensitive carriers have been used to load anticancer drugs to accelerate their release during PTT therapy.[9,10] Such strategies can not only combine the effects of PTT and chemotherapy but also control the release of anticancer drugs, thus resulting in an effective synergistic effect.[11]

PTT agents and anticancer drugs have been coloaded in thermosensitive nanocarriers to prepare composite nanoparticles with a synergistic effect.[12,13] Thermosensitive liposomes prepared from thermosensitive lipids, such as 1,2-dipalmitoyl-*sn*-glycero-3-phosphocholine (DPPC), are useful carriers for these types of systems.[14,15] DPPC has a phase transition temperature near 42 °C; thus DPPC liposomes can release encapsulated drugs near or above 42 °C.[16,17] The composite nanoparticles are administered through intravenous injection and circulate in the vessels to reach the cancer cells.[18] However, the therapeutic outcomes of administering composite nanoparticles *via* intravenous injection are very limited due to the rapid clearance of the injected nanoparticles by the immune system and the side effects of high dosages.[19,20] To overcome these drawbacks, the use of porous scaffolds or hydrogels as effective local delivery carriers has been reported.[21–26] PTT agents have been hybridized with polymers or ceramics to construct photothermal composite scaffolds.[27,28] Furthermore, PTT agents and anticancer drug-loaded thermosensitive liposomes have been incorporated into

[a]*Research Center for Functional Materials, National Institute for Materials Science, 1-1 Namiki, Tsukuba, Ibaraki 305-0044, Japan. E-mail: Guoping.CHEN@nims.go.jp; Fax: +81-29-860-4673; Tel: +81-29-860-4496*

[b]*Department of Materials Science and Engineering, Graduate School of Pure and Applied Sciences, University of Tsukuba, 1-1-1 Tennodai, Tsukuba, Ibaraki 305-8577, Japan*

[c]*Graduate School of Life and Environmental Science, University of Tsukuba, 1-1-1 Tennodai, Tsukuba, Ibaraki 305-8572, Japan*

† Electronic supplementary information (ESI) available. See DOI: https://doi.org/10.1039/d2bm01155g

polymer porous scaffolds to form composite scaffolds with good photothermal conversion and controllable drug release properties.[29]

These synergistic composite scaffolds can generate a strong PTT effect under NIR laser irradiation for the ablation of cancer cells in or near the scaffolds.[30] Moreover, they can kill cancer cells that are outside the scaffolds through the release of anticancer drugs, which can be accelerated by NIR laser irradiation.[31,32] However, the high PPT temperature is only required for the ablation of cancer cells in the beginning. During the subsequent chemotherapy, which depended on the released anticancer drugs, a mild hyperthermia environment is desirable to trigger the release of anticancer drugs without hyperthermia-induced damage to normal cells. Therefore, the stepwise control of hyperthermia temperatures at a high level for hyperthermia therapy and a low level for afterward chemotherapy is needed.

Hence, in this study, a stepwise photothermal therapy and chemotherapy platform was established by using photothermal composite scaffolds comprising a stable PPT agent and a biodegradable PPT agent (Scheme 1). Gold nanorods (AuNRs) were used as the stable PPT agent, and black phosphorus nanosheets (BPNSs) were used as the biodegradable PTT agent because BPNSs can be degraded into nontoxic phosphonate and phosphate ions after implantation.[33] Both AuNRs and BPNSs have good photothermal conversion properties and biocompatibility.[34–37] Before the degradation of BPNSs, the incorporated AuNRs and BPNSs could generate a high hyperthermia temperature. After the degradation of BPNSs, the stable AuNRs could generate a mild hyperthermia temperature to trigger the release of anticancer drugs. The hyperthermal composite scaffolds were prepared by hybridizing AuNRs, BPNSs, Dox-loaded DPPC liposomes, polyglutamic acid (PGA) and gelatin. The *in vitro* and *in vivo* experiments demonstrated that the composite scaffolds had a synergistic effect of PTT and chemotherapy in the early stage and a chemotherapy effect in the late stage. The chemotherapeutic effect in the late stage could be enhanced by the accelerated release of Dox, which was controlled by the mild hyperthermia environment. Furthermore, the composite scaffolds could support the proliferation of stem cells after the complete release of Dox, which should be beneficial for guiding new tissue regeneration after the complete eradication of cancer cells. The composite scaffolds should provide a good platform for synergistic cancer therapy.

## Materials and methods

### Synthesis of gold nanorods and black phosphorus nanosheets

AuNRs were synthesized by a seed-growth method.[32] The seeds were prepared by a quick reduction of $HAuCl_4$ with $NaBH_4$ and stabilization with hexadecyltrimethylammonium bromide (CTAB). The seed solution (0.48 mL) was mixed with 10 mL of 0.01 M $HAuCl_4$, 4 mL of 1 M HCl, 2.20 mL of 10 mM $AgNO_3$, 1.6 mL of 0.1 M ascorbic acid and 150 mL of 0.1 M CTAB to synthesize the AuNRs. The AuNRs were observed with transmission electron microscopy (TEM, JEOL 2011F, Japan). The longitudinal length and transverse length of the AuNRs were measured from the corresponding TEM images using the ImageJ software (National Institutes of Health, Bethesda, MD, USA). Every 50 nanoparticles from three images were analyzed. The UV-visible spectrum of the AuNRs was measured with a UV-2600 UV-visible spectrophotometer (Shimadzu Corp., Japan).

BPNSs were exfoliated by liquid phase exfoliation based on a previous method with slight modification.[38,39] Briefly, 100 mg of bulk black phosphorus (BBP, Smart-elements, Vienna, Austria) was ground to a fine powder under protection with argon gas in a glovebox, and then 2 mL of *N*-methyl-2-pyrrolidone (NMP) was mixed with the BBP powder. The mixture solution was ground again, dispersed in 98 mL of NMP and further exfoliated by sonication in an ice bath for 24 h using a power of 650 W under argon gas protection. Afterward, the brown dispersion solution was sonicated overnight using an ultrasonic bath sonicator and centrifuged using a centrifugation machine (Hitachi Koki, Hitachinaka, Japan) at 4000 rpm for 15 min to separate the large and unexfoliated particles. The supernatant of the sample was collected and centrifuged for another 60 min at 20 000 rpm. Finally, the pellet of the centrifuged sample was collected and resuspended in

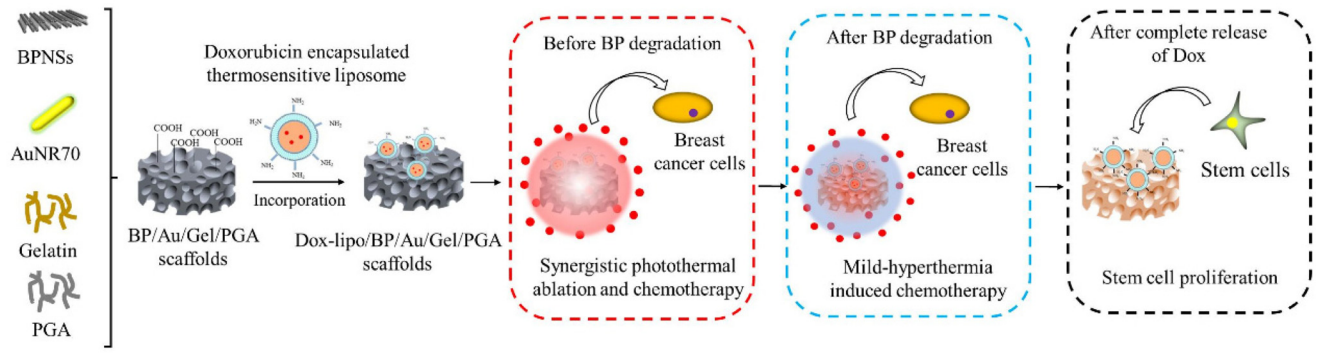


**Scheme 1** Preparation of Dox-lipo/BP/Au/Gel/PGA composite scaffolds and their stepwise therapeutic effects before and after BP degradation and promotive effect on stem cell proliferation after complete release of Dox.

100 mL of NMP solution and stored in a dark argon glovebox for further experiments.

### Preparation of composite scaffolds of AuNRs, BPNSs, gelatin and PGA

The composite scaffolds of AuNRs, BPNSs, gelatin and PGA (BP/Au/Gel/PGA) were prepared by hybridizing these four components (Scheme 1). Gelatin and PGA were dissolved in Milli-Q water. The BPNSs were washed with Milli-Q water thrice to completely remove NMP and resuspended in Milli-Q water. First, the gelatin solution was mixed with the PGA solution at room temperature. Then, the AuNRs and BPNSs was added to the gelatin/PGA mixture solution upon sonication at room temperature for 15 min. The final concentrations of AuNRs, BPNSs, gelatin and PGA were 0.3 mM, 200 μg $mL^{-1}$, 4 (wt/v)% and 0.4 (wt/v)%, respectively. The mixture solution was added to a silicone mold at room temperature, followed by freezing at −80 °C for 12 h. Finally, the frozen constructs were freeze-dried. After freeze-drying, the constructs were washed with ethanol and cross-linked with 50.0 mM EDC and 20.0 mM NHS dissolved in a mixture solution of ethanol and 0.1% (wt/vol) MES with a series of ethanol/water ratios of 95/5, 90/10 and 85/5 (v/v), each for 8 h. After cross-linking, the BP/Au/Gel/PGA composite scaffolds were washed with Milli-Q water 8 times. Finally, the composite scaffolds were freeze-dried and stored under argon protection. As controls, Au/Gel/PGA and Gel/PGA composite scaffolds were prepared by the above-described method with or without the addition of AuNRs. The pore structures of the Gel/PGA, Au/Gel/PGA and BP/Au/Gel/PGA composite scaffolds were observed *via* scanning electron microscopy (SEM, Hitachi S-4800, Japan).

### Preparation of Dox-encapsulated liposomes

1,2-Dipalmitoyl-*sn-glycero*-3-phosphocholine (DPPC), cholesterol (Chol) and 1,2-distearoyl-*sn-glycero*-3-phosphoethanolamine-*N*-[amino(polyethyleneglycol)-2000] (ammonium salt) (DSPE-PEG-$NH_2$) were used to prepare the Dox-encapsulated DPPC/Chol/DSPE-PEG-$NH_2$ liposomes by a thin-film hydration method.[29] First, 5 mL of chloroform was added to a 50 mL round-bottle flask for rinsing, followed by chloroform removal and drying the flask before adding lipid solution. Then, 600 μL of DPPC (5 mg $mL^{-1}$), 80 μL of cholesterol (5 mg $mL^{-1}$) and 320 μL of DSPE-PEG2000-$NH_2$ (5 mg $mL^{-1}$) in a chloroform/methanol (v/v = 9 : 1) solvent mixture were mixed in a clean flask. The final volume of the mixture was 1 mL, and the molar ratio of DPPC : Chol : DSPE-PEG2000-$NH_2$ was 7 : 2 : 1. Then, the flask was connected to a rotary evaporator and immersed in a water bath that was preheated to 45 °C. The chloroform/methanol solvent mixture was gradually evaporated under vacuum and rotation. A thin film was formed after removing the solvent. Then, the flask was placed in a vacuum dryer overnight for further drying. Finally, the lipid thin film was hydrated to prepare the liposomes. Water bath sonication was used for hydration. Dox was encapsulated into liposomes during the hydration process. Dox solution in PBS (1 mL, 1 mg $mL^{-1}$) was added to the flask to wet the lipid thin film at room temperature for 30 min. The hydrated thin film was sonicated at 60 °C for 30 min. After sonication, the hydrated thin film was extruded 21 times at 60 °C through a polycarbonate membrane with a pore size of 200 nm. The extruded solution was centrifuged at 20 000 rpm for 15 min and washed with PBS. After centrifugation, the Dox-encapsulated liposome precipitant was resuspended in PBS solution and stored at 4 °C.

The size distribution of the dox-encapsulated liposomes was measured by dynamic light scattering (DLS; Otsuka Electronics Co., Ltd, Japan).

### Preparation of liposome-incorporated composite scaffolds

The Dox-encapsulated liposomes were incorporated into the Au/Gel/PGA and BP/Au/Gel/PGA composite scaffolds to prepare Dox-lipo/Au/Gel/PGA and Dox-lipo/BP/Au/Gel/PGA composite scaffolds, respectively (Scheme 1). The carboxyl groups of the Au/Gel/PGA and BP/Au/Gel/PGA scaffolds were activated and conjugated with the amino groups of the Dox-encapsulated liposomes. In brief, the scaffolds were cut into round disks with a diameter of 6 mm and a thickness of 1 mm. The Au/Gel/PGA and BP/Au/Gel/PGA scaffold discs were immersed in EDC/NHS aqueous solution (50 mM/20 mM) at room temperature for 6 h to activate the carboxyl groups. After activation, the Au/Gel/PGA and BP/Au/Gel/PGA scaffold discs were washed with PBS. After removing the excess solution in the activated scaffolds, 30 μL of the Dox-encapsulated liposome solution with a Dox concentration of 1 mg $mL^{-1}$ was added to each of the scaffold discs and reacted at room temperature for 12 h under shaking. After the reaction, the scaffold discs were washed with PBS three times to remove unbound liposomes to obtain the Dox-lipo/Au/Gel/PGA and Dox-lipo/BP/Au/Gel/PGA composite scaffolds. Their pore structures were observed with SEM.

The amount of Dox loaded in the Dox-lipo/BP/Au/Gel/PGA composite scaffolds was measured using a fluorescence spectrophotometer.[29] The Dox-lipo/BP/Au/Gel/PGA composite scaffolds were treated with a solvent mixture of chloroform/methanol (v/v = 1/1) to destroy the liposomes in the scaffolds. The fluorescence of the mixture solution was measured at an excitation/emission wavelength of 470/560 nm. The amount of Dox in the mixture solution was calculated based on a standard curve. The loading efficiency of Dox in the composite scaffolds was calculated by dividing the Dox amount in the composite scaffolds with the Dox amount in the liposomes used for the preparation of the composite scaffolds. Three samples were used for the measurement.

### Photothermal conversion property of composite scaffolds

The photothermal conversion properties of the Gel/PGA, Au/Gel/PGA, BP/Au/Gel/PGA, Dox-lipo/Au/Gel/PGA and Dox-lipo/BP/Au/Gel/PGA composite scaffolds were investigated during NIR laser irradiation. The scaffolds were cut into discs ($\Phi$ 6 mm × $H$ 1 mm), and each disc was hydrated with 30 μL of Milli-Q water. The hydrated scaffold discs were irradiated with an 805 nm laser with different intensities (1.3 and 1.6 W $cm^{-2}$) for 10 min. The temperature of each hydrated scaffold disc was

 

recorded every 30 s during laser irradiation using an electronic thermometer (As one Corp., Osaka, Japan). The spot size of the laser beam was 8 × 6 mm. The photothermal conversion efficiency ($\eta$) was calculated based on a heating–cooling circulation method, which is shown in the ESI,† according to a previously reported method.[40]

### Dox release from Dox-loaded composite scaffolds

NIR laser-induced Dox release from the Dox-lipo/Au/Gel/PGA and Dox-lipo/BP/Au/Gel/PGA composite scaffolds was investigated by periodically irradiating the scaffold discs during incubation in PBS at 37 °C. Each disc of the composite scaffolds was immersed and incubated in 500 μL PBS at 37 °C under shaking. After 24 h of incubation, the scaffold discs were removed and irradiated with an NIR laser at an intensity of 1.6 W $cm^{-2}$ for 10 min. The irradiation was conducted periodically after every 24 h of incubation. After irradiation, the discs were returned for continued incubation. At the time points before and after every periodical irradiation, 100 μL of PBS was collected, and another 100 μL of fresh PBS was added. The amount of released Dox in the collected samples was measured, and the cumulative release of Dox was calculated. The release of Dox from the composite scaffolds during incubation at a constant temperature of 37 °C was also investigated by the same method but without laser irradiation. Triplicate samples were used for all of these measurements.

### *In vitro* anticancer effect of the composite scaffolds

The *in vitro* therapeutic effect of the composite scaffolds was investigated by culturing breast cancer cells in the scaffolds with or without laser irradiation. Scaffold discs ($\Phi$ 6 mm × $H$ 1 mm) were sterilized with 70% ethanol and washed with PBS thrice. The sub-cultured MDA-MB-231-Luc cells (JCRB, Osaka, Japan) were collected by trypsin treatment and resuspended in DMEM serum medium at a concentration of $5 \times 10^6$ cells per mL. A total of 20 μL of the cell suspension was seeded on one side of the scaffold discs and cultured in DMEM serum medium in a humidified incubator (5% $CO_2$, 37 °C) for 6 h. After 6 h of incubation, the scaffold discs were turned upside down, and another side was seeded with another 20 μL of cell suspension solution and cultured for 6 h. The MDA-MB-231-Luc cells were also seeded in the bottom wells of 24-well transwell plates (Thermo Fisher Scientific Inc. Japan) and cultured for 6 h. Then, the cell/scaffold constructs were transferred into the culture inserts and cocultured with the cells seeded in the bottom wells. The medium in each well was 1 mL in total. The culture inserts contained a PET membrane with a pore size of 8 μm that ensured the diffusion of the released Dox. After culture for 12 h, the cell/scaffold constructs in the inserts were taken out and irradiated with an 805 nm laser at an intensity of 1.6 W $cm^{-2}$ for 10 min. After laser irradiation, the cell/scaffold discs were immediately returned to the culture inserts. Then, the cell/scaffold constructs were cultured for another 72 h. A live/dead staining kit (Dojindo, Japan) was used to visualize live and dead cells in the scaffolds. The cell/scaffold constructs were washed with PBS and stained with calcein-AM and propidium iodide in serum-free medium for 15 min. The stained cells were observed with fluorescence microscopy (Olympus, Japan). The WST-1 assay was used to evaluate the viability of MDA-MB-231-Luc cells cultured in the scaffold discs and the bottom wells of the 24-well transwell plates. The cell/scaffold constructs were transferred to the wells of new 24-well plates containing 1 mL of the culture medium. The bottom wells of the 24-well transwell plates were changed with 1 mL fresh culture medium. Then, 400 μL of the WST-1 reagent diluted with medium (1 : 10) was added to each well, and the cells were cultured for another 3 h. The absorbance of the WST-1 solution at 440 nm was measured using a microplate reader (Benchmark Plus, Bio-Rad, Hercules, CA, USA). Triplicate samples were used for each measurement.

### *In vivo* anticancer effect of the composite scaffolds

The animal experimental procedures were approved by the Animal Experiments Committee of the National Institute for Materials Science, and the experiments were conducted according to the committee guidelines. The MDA-MB-231-Luc cells were seeded in discs of the Gel/PGA, Au/Gel/PGA, BP/Au/Gel/PGA, Dox-lipo/Au/Gel/PGA and Dox-lipo/BP/Au/Gel/PGA composite scaffolds ($\Phi$ 6 mm × $H$ 1 mm) as described above. The Gel/PGA composite scaffolds without AuNRs, BPNSs or Dox were cut into rings with an inner diameter of 6 mm and an outer diameter of 10 mm. The thickness of the Gel/PGA scaffold rings was 2 mm. The MDA-MB-231-Luc cells were seeded on both sides of the Gel/PGA scaffold rings by adding 50 μL of the cell suspension solution ($2 \times 10^6$ cells per mL) on each side of the scaffold rings and culturing in DMEM serum medium for 6 h during each cell seeding. After another 12 h of culture, the cell/scaffold discs were placed in the inner openings of the cell/scaffold rings and subcutaneously implanted together in 6-week-old female BALB/c nude mice. After implantation for 1 d, the implanted sites were irradiated with an 805 nm laser at an intensity of 1.6 W $cm^{-2}$ for 10 min. During laser irradiation, IR thermal photographs and temperatures were recorded with an IR camera. One day after the first irradiation, the implanted sites were irradiated for the second time under the same conditions as the first irradiation. An *in vivo* vision system (IVIS, Lumina III, PerkinElmer, MA, Japan) was used to examine the viability of the MDA-MB231-Luc cells in the scaffolds before laser irradiation and 1 d after the first and second laser irradiation. D-Luciferin (Wako Corp. Japan) solution was administered by intraperitoneal injection at the designated examination time points. After 10 min, the mice were anesthetized with 2% isoflurane and imaged with an IVIS. Three mice were used for each scaffold group.

For a long period of the implantation experiment, the MDA-MB-231-Luc cells were seeded in discs of Dox-lipo/BP/Au/Gel/PGA composite scaffolds ($\Phi$ 6 mm × $H$ 1 mm), plugged in Gel/PGA scaffold rings seeded with breast cancer cells, and implanted as described above. After implantation for 13 d, the implanted sites were irradiated with an 805 nm laser at an intensity of 1.6 W $cm^{-2}$ for 10 min. In the following 3 days, the implanted sites were irradiated once each day (totally 4 times

irradiation). The irradiation was conducted four times. The IVIS was used to examine the viability of the MDA-MB-231-Luc cells in the scaffolds after implantation for 1 d and 13 d. IVIS imaging was also conducted before each laser irradiation and 17 d after implantation.

### Culture of hMSCs in composite scaffolds after drug release

The influence of the Dox-lipo/BP/Au/Gel/PGA composite scaffolds after the complete release of the loaded Dox on the viability of human bone marrow-derived mesenchymal stem cells (hMSCs) was evaluated. The scaffolds were cut into round disks ($\Phi$ 6 mm × $H$ 1 mm). Before cell seeding, the composite scaffolds were irradiated with an NIR laser 10 times to completely release the loaded Dox. After 10 times laser irradiation, almost no released Dox was detected from the scaffold discs. Then, the laser-irradiated scaffold discs were washed with PBS and seeded with hMSCs. The hMSCs were purchased from Lonza (Walkersville MD, USA) and sub-cultured in MSCBM medium (Lonza, Switzerland). The sub-cultured hMSCs were harvested by trypsin treatment and resuspended in DMEM to prepare a cell suspension solution at a cell concentration of $4.0 \times 10^6$ cells per mL. A total of 20 μL of the cell suspension solution was seeded on one side of the scaffolds. After 6 h of culture, the other side of the scaffolds was seeded with 20 μL of the cell suspension solution. After 6 h of culture, the hMSC/scaffold constructs were transferred into cell culture dishes for further culturing. The culture medium was changed every 3 d. After culturing for 3 d, the viability of hMSCs in the composite scaffolds was examined by live/dead staining. After culturing for 3, 5 and 7 d, cell proliferation was determined by measuring the amount of DNA in the scaffolds. The hMSC/scaffold constructs were washed with PBS thrice and pure water once, followed by freeze-drying. Then, the freeze-dried hMSC/scaffold constructs were digested with 400 μg $mL^{-1}$ papain solution containing 5 mM EDTA and 5 mM L-cysteine in 0.1 M phosphate buffer (pH 6.0). The amount of DNA in the digest solution was measured by Hoechst 33258 dye (Sigma Aldrich, USA) using a fluorescence spectrometer (FP8500, JASCO, Japan). Triplicate samples were used for DNA quantification.

### Statistical analysis

All quantitative experiments were performed in triplicate ($n$ = 3). All the results are expressed as the means ± standard deviations. Statistical analysis of the experimental data was performed by using one-way analysis of variance using the Origin Pro software (8.0). The $p$ value was used to determine the level of significance: $^*P < 0.05$, $^{**}P < 0.01$ and $^{***}P < 0.001$.

## Results and discussion

### Characterization of AuNRs, BPNSs and Dox-encapsulated liposomes

The morphologies and absorbances of AuNRs and BPNSs were characterized and confirmed by TEM and UV-visible spectrophotometry (Fig. 1). The AuNRs were synthesized based on a seed-growth method. The rod-like shape and size of the AuNRs were confirmed by TEM images. The longitudinal length and transverse length of the AuNRs were 69.7 ± 3.1 nm and 13.6 ± 1.9 nm, respectively. The spectrum of the AuNRs showed a strong and sharp absorbance peak in the NIR region, indicating a strong photothermal effect. The BPNSs showed a sheet-like structure, which could be attributed to the breakage of weak van der Waals forces between the layers of BP during exfoliation. The spectrum of the BPNSs showed a broad absorbance in the UV to NIR region, which suggested that BPNSs had the potential to be used as a PTT agent. The size of the Dox-encapsulated liposomes was analyzed by dynamic light scattering (Fig. S1†). The mean size of the liposomes was 230.2 ± 58.7 nm.

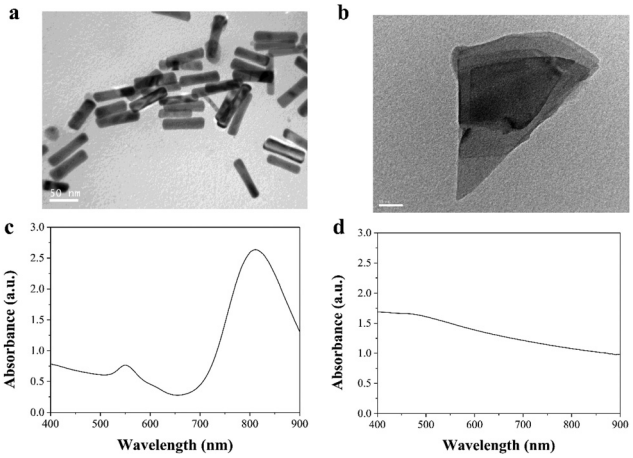


Fig. 1 Characterization of AuNRs and BPNSs. Transmission electron microscopy images of (a) AuNRs and (b) BPNSs. UV-vis spectra of (c) AuNRs and (d) BPNSs.

### Characterization of the composite scaffolds

The Gel/PGA, Au/Gel/PGA and BP/Au/Gel/PGA composite scaffolds were prepared with or without AuNRs and BPNSs. Dox-encapsulated thermosensitive liposomes were incorporated into the composite scaffolds through the reaction between the amino groups in the liposomal membrane and the carboxyl groups in the scaffolds. SEM observation showed that all these composite scaffolds had similar porous structures (Fig. 2a–c). The pores were formed after freezing and freeze-drying. The incorporation of the Dox-encapsulated thermosensitive liposomes had no influence on the porous structures of the scaffolds (Fig. 2d and e). The loading efficiency of Dox in the composite scaffolds was 48.6 ± 4.2%.

The photothermal conversion effects of the composite scaffolds were investigated by NIR laser irradiation at an intensity of 1.3 W $cm^{-2}$ and 1.6 W $cm^{-2}$ for 10 min. The Gel/PGA composite scaffolds showed no evident photothermal conversion effects during NIR laser irradiation (Fig. 3a). After 10 min of irradiation, the temperature of the Gel/PGA composite scaffolds was lower than 32.3 °C. In contrast, the composite scaffolds containing AuNRs and BPNSs showed a large temp-

 

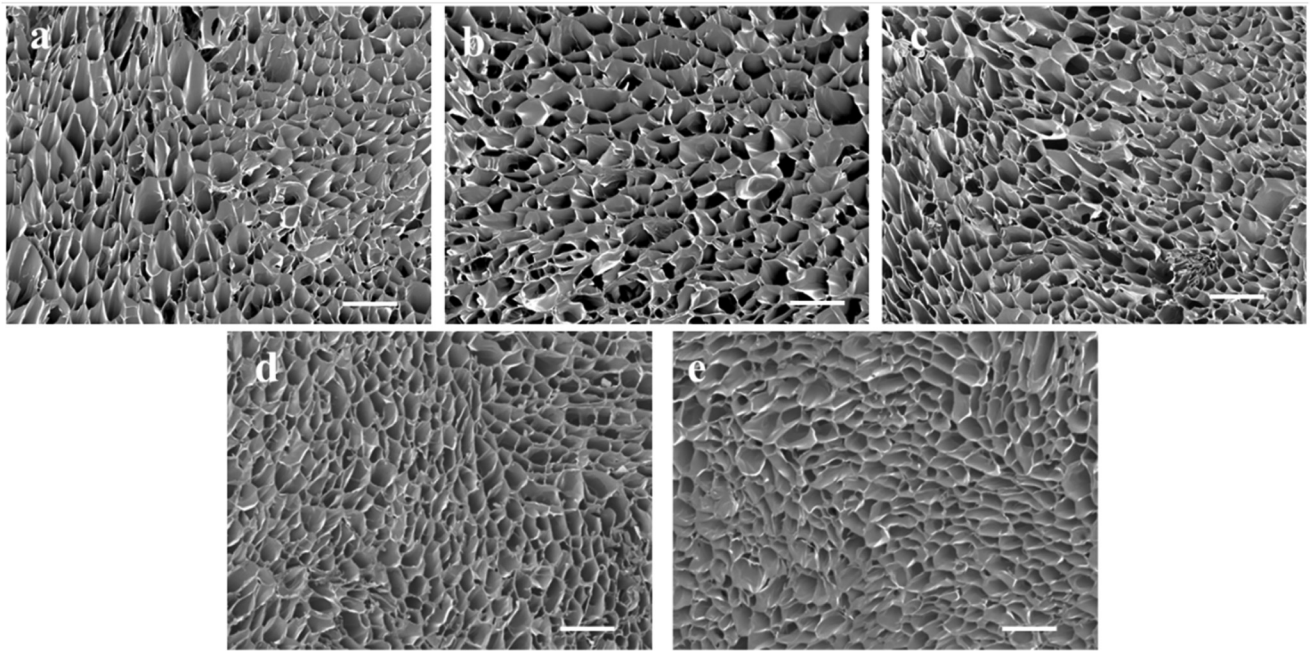


**Fig. 2** Scanning electron microscopy images of (a) Gel/PGA, (b) Au/Gel/PGA, (c) BP/Au/Gel/PGA, (d) Dox-lipo/Au/Gel/PGA and (e) Dox-lipo/BP/Au/Gel/PGA composite scaffolds. Scale bar: 500 μm.

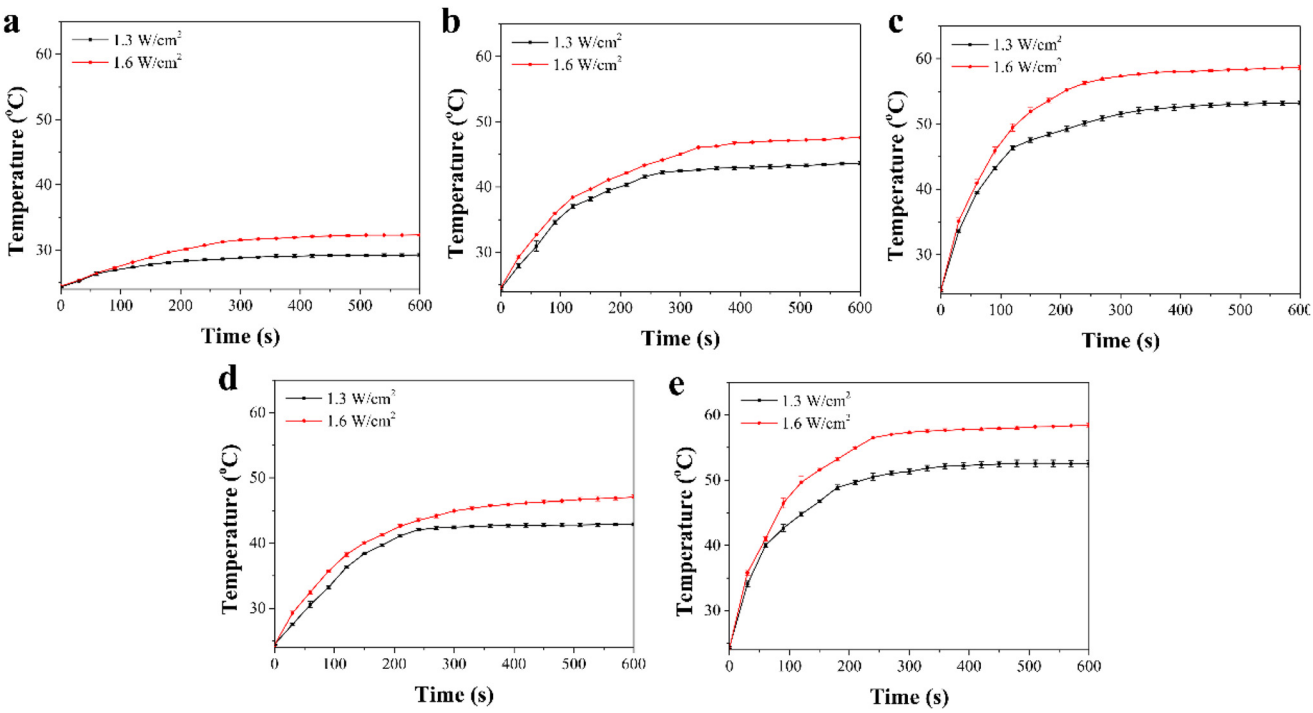


**Fig. 3** Heating curves of (a) Gel/PGA, (b) Au/Gel/PGA, (c) BP/Au/Gel/PGA, (d) Dox-lipo/Au/Gel/PGA and (e) Dox-lipo/BP/Au/Gel/PGA composite scaffolds during NIR laser irradiation for 10 min at intensities of 1.3 and 1.6 W $cm^{-2}$. Data are presented as the means ± S.D ($n$ = 3).

erature increase (Fig. 3b–e). The temperature change increased with increasing laser intensity and irradiation time. After 10 min of irradiation with the 1.6 W $cm^{-2}$ NIR laser, the temperatures of the Au/Gel/PGA, BP/Au/Gel/PGA, Dox-lipo/Au/Gel/PGA and Dox-lipo/BP/Au/Gel/PGA composite scaffolds reached 47.6, 58.6, 47.0 and 58.4 °C, respectively. The incorporation of AuNRs and BPNSs endowed the composite scaffolds with photothermal conversion properties. The co-loading of AuNRs

and BPNSs resulted in better photothermal conversion capacity than the loading of AuNRs alone. The incorporation of Dox-encapsulated liposomes did not affect the photothermal convention property of the composite scaffolds. The photothermal conversion efficiency of the Dox-lipo/BP/Au/Gel/PGA composite scaffolds was 39.8%, which was calculated by a heating–cooling circulation (Fig. S2†).

### Laser-induced release of Dox from composite scaffolds

The release profiles of Dox from the Dox-lipo/Au/Gel/PGA and Dox-lipo/BP/Au/Gel/PGA composite scaffolds were investigated by periodic laser irradiation (Fig. 4). The results showed that Dox was slowly released from the Dox-lipo/Au/Gel/PGA and Dox-lipo/BP/Au/Gel/PGA composite scaffolds during incubation at a constant temperature of 37 °C without laser irradiation. When the composite scaffolds were irradiated with 1.6 W $cm^{-2}$ NIR laser for 10 min, Dox release dramatically increased. Dox release was accelerated during laser irradiation but slowed down when the laser irradiation was turned off. Therefore, Dox release from the composite scaffolds could be regulated by laser irradiation. After 10 times laser irradiation, the amount of released Dox remained almost unchanged even after further laser irradiation. The accelerated release of Dox should be due to the laser irradiation-induced high temperatures of the composite scaffolds, which were higher than the liposome phase transition temperature. The temperatures of the Dox-lipo/Au/Gel/PGA and Dox-lipo/BP/Au/Gel/PGA composite scaffolds increased to 47.0 and 58.4 °C after 1.6 W $cm^{-2}$ laser irradiation for 10 min (Fig. 3d and e). When laser irradiation ceased, the temperatures in the composite scaffolds returned to the incubation buffer temperature (37 °C), which was lower than the liposome phase transition temperature. Dox release was subsequently slowed. After 10 times laser irradiation, most of the encapsulated Dox was released, and the amount of residual Dox in the liposomes was low. The decreased concentration of Dox in the liposomes should weaken the diffusion of residual Dox through the liposome membranes, thereby slowing the release of residual Dox even under laser irradiation.

### *In vitro* therapeutic effect of composite scaffolds

The *in vitro* therapeutic effects of the composite scaffolds were evaluated by using transwell plates. MDA-MB-231-Luc breast cancer cells were cultured in both the composite scaffolds that were placed in the inserts and the bottom wells of plates. The cells in the scaffolds should be affected by the scaffold temperature change and the released Dox, while the cells in the bottom wells should be affected by the released Dox, not the scaffold temperature, because the cells in the bottom wells were separated from the scaffolds by the insert membrane.

For the composite scaffolds without Dox loading (Gel/PGA, Au/Gel/PGA and BP/Au/Gel/PGA composite scaffolds), live/dead staining showed that no dead cells were observed in these three composite scaffolds without laser irradiation (Fig. 5a). After laser irradiation, no dead cells were detected in the Gel/PGA composite scaffolds, while a small number of dead cells were observed in the Au/Gel/PGA composite scaffolds and a large number of dead cells were observed in the BP/Au/Gel/PGA composite scaffolds. The WST-1 assay showed that the viability of cells cultured in the Gel/PGA composite scaffolds did not change with or without laser irradiation (Fig. 5b). However, cell viability in the Au/Gel/PGA and BP/Au/Gel/PGA composite scaffolds significantly decreased after laser irradiation. Cell viability in the BP/Au/Gel/PGA composite scaffolds was lower than that in the Au/Gel/PGA composite scaffolds after laser irradiation. The higher temperature of the BP/Au/Gel/PGA composite scaffolds killed more cancer cells compared with the Au/Gel/PGA composite scaffolds after laser

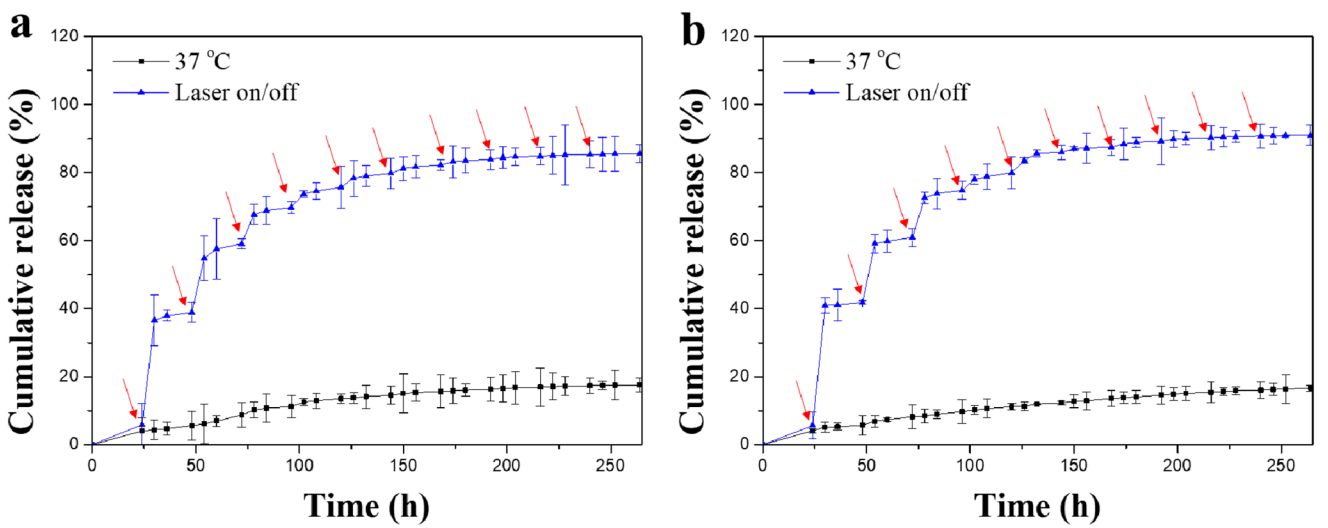


Fig. 4 Release profiles of Dox from (a) Dox-lipo/Au/Gel/PGA and (b) Dox-lipo/BP/Au/Gel/PGA composite scaffolds in PBS at a constant temperature of 37 °C and during a periodic on/off of 1.6 W $cm^{-2}$ NIR laser irradiation for 10 min. The arrows indicate the time point when the NIR laser irradiation started. Data are presented as the means ± S.D ($n$ = 3).

 

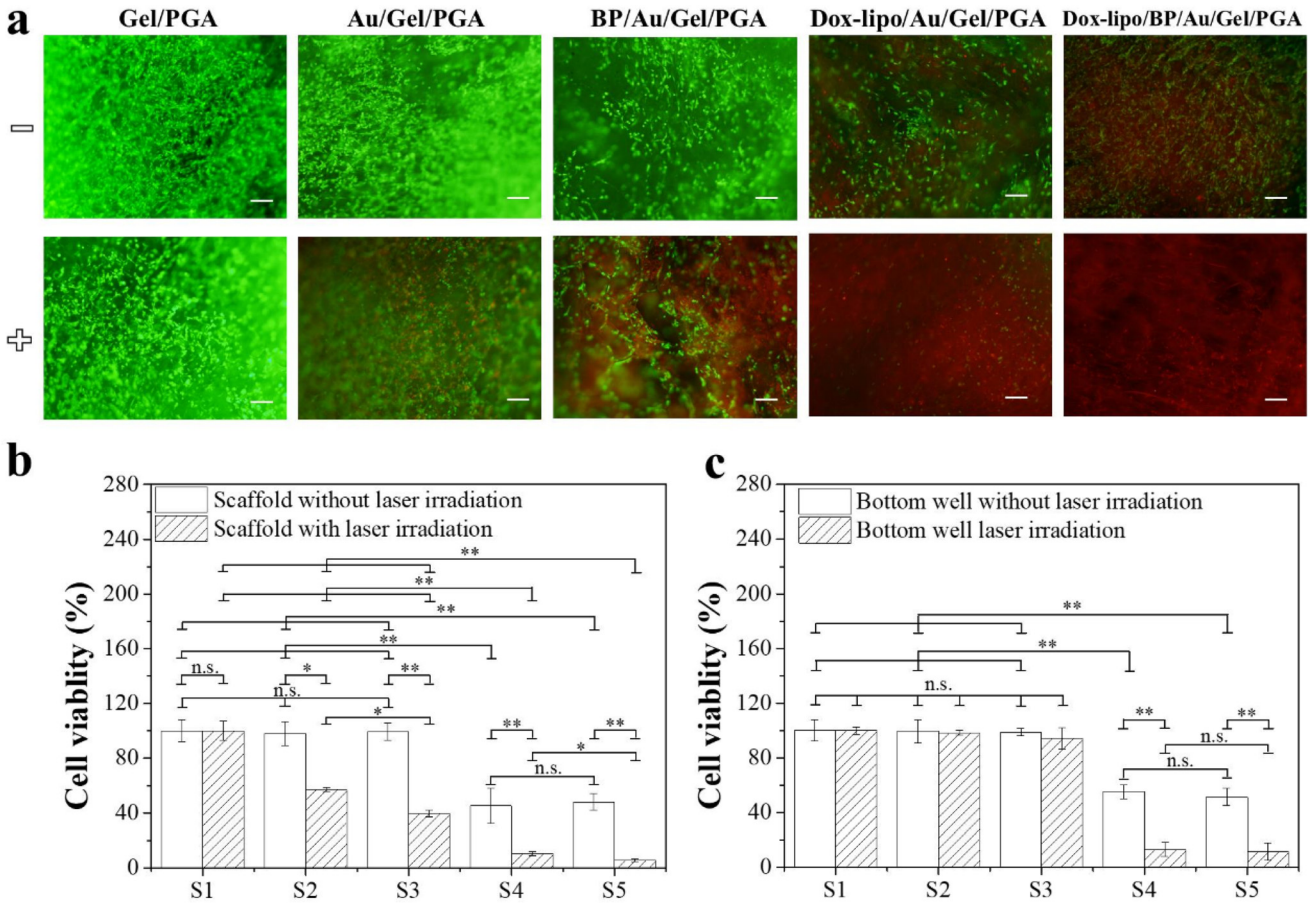


**Fig. 5** (a) Live/dead staining of breast cancer cells cultured in the composite scaffolds without (–) or with (+) NIR laser irradiation (1.6 W $cm^{-2}$, 10 min). Viable cells were stained green, while dead cells were stained red. Scale bar: 200 μm. Quantified viability of breast cancer cells cultured in (b) the composite scaffolds or in (c) the bottom wells of transwell plates covered with inserts containing the composite scaffolds with or without NIR laser irradiation (1.6 W $cm^{-2}$, 10 min). S1: Gel/PGA; S2: Au/Gel/PGA; S3: BP/Au/Gel/PGA; S4: Dox-lipo/Au/Gel/PGA; and S5: Dox-lipo/BP/Au/Gel/PGA composite scaffolds. Data are presented as the means ± S.D ($n$ = 3). Significant difference: *$p$ < 0.05; **$p$ < 0.01; ***$p$ < 0.001. N.S. = no significant difference.

irradiation. The viability of cells cultured in the bottom wells under the inserts containing the Gel/PGA, Au/Gel/PGA and BP/Au/Gel/PGA composite scaffolds did not change with or without laser irradiation (Fig. 5c). The results indicated that the temperature changes of the composite scaffolds induced by laser irradiation could kill the cancer cells in the scaffolds placed in the inserts but had no influence on the cells cultured on the bottom wells.

For the Dox-loaded composite scaffolds (Dox-lipo/Au/Gel/PGA and Dox-lipo/BP/Au/Gel/PGA), some dead cells were observed before laser irradiation (Fig. 5a). After laser irradiation, more dead cells were observed in these two composite scaffolds. The WST-1 assay indicated that cell viability in the Dox-lipo/Au/Gel/PGA and Dox-lipo/BP/Au/Gel/PGA composite scaffolds was significantly lower than those in the Gel/PGA, Au/Gel/PGA and BP/Au/Gel/PGA composite scaffolds both before and after laser irradiation (Fig. 5b). The breast cancer cells in the Dox-lipo/Au/Gel/PGA and Dox-lipo/BP/Au/Gel/PGA composite scaffolds were killed by both the laser irradiation-induced temperature increase and the released Dox. The viability of cells cultured in the bottom wells under the Dox-lipo/Au/Gel/PGA and Dox-lipo/BP/Au/Gel/PGA composite scaffolds was significantly lower than that of cells cultured in the bottom well under the composite scaffolds without Dox loading before laser irradiation (Fig. 5c). The slowly released Dox from the Dox-loaded composite scaffolds before laser irradiation killed some breast cancer cells. After laser irradiation, the cell viability in the bottom wells under the Dox-lipo/Au/Gel/PGA and Dox-lipo/BP/Au/Gel/PGA composite scaffolds was further decreased. This should be due to the killing of more breast cancer cells by the accelerated release of Dox that was induced by laser irradiation.

The *in vitro* therapeutic effects of the composite scaffolds can be summarized as follows. First, the Gel/PGA composite scaffolds without the incorporation of either PTT agents or Dox had no influence on cell viability with or without laser irradiation. Second, without laser irradiation, the Dox-loaded composite scaffolds (Dox-lipo/Au/Gel/PGA and Dox-lipo/BP/Au/Gel/PGA) killed some breast cancer cells in the scaffolds or in the bottom wells, while the composite scaffolds without Dox

loading had no influence on cell viability. Third, with laser irradiation, the composite scaffolds incorporated with AuNRs or BPNSs/AuNRs killed some breast cancer cells in the scaffolds but not the cells in the bottom wells, while the composite scaffolds loaded with both PTT agents and Dox killed cells in both the scaffolds and the bottom wells. Fourth, the composite scaffolds loaded with both PTT agents and Dox could kill more cells after laser irradiation.

### *In vivo* therapeutic effect of composite scaffolds

The therapeutic effects of the Gel/PGA, Au/Gel/PGA, BP/Au/Gel/PGA, Dox-lipo/Au/Gel/PGA and Dox-lipo/BP/Au/Gel/PGA composite scaffolds were further investigated *in vivo* by using nude mice. The MDA-MB-231-Luc breast cancer cells were cultured in composite scaffold discs and Gel/PGA scaffold rings. The cell/scaffold discs were plugged into the Gel/PGA scaffold rings and implanted together (Fig. 6a). The cells in the cells/scaffold discs should be affected by both the temperature of the scaffolds and the released Dox. On the other hand, the breast cancer cells in the Gel/PGA scaffold rings should be affected only by the released Dox, not by the scaffold temperature, which might mimic the behavior of metastatic cancer cells.

The implanted cell/scaffold constructs were irradiated with a 1.6 W $cm^{-2}$ NIR laser for 10 min (Fig. 6a). During laser

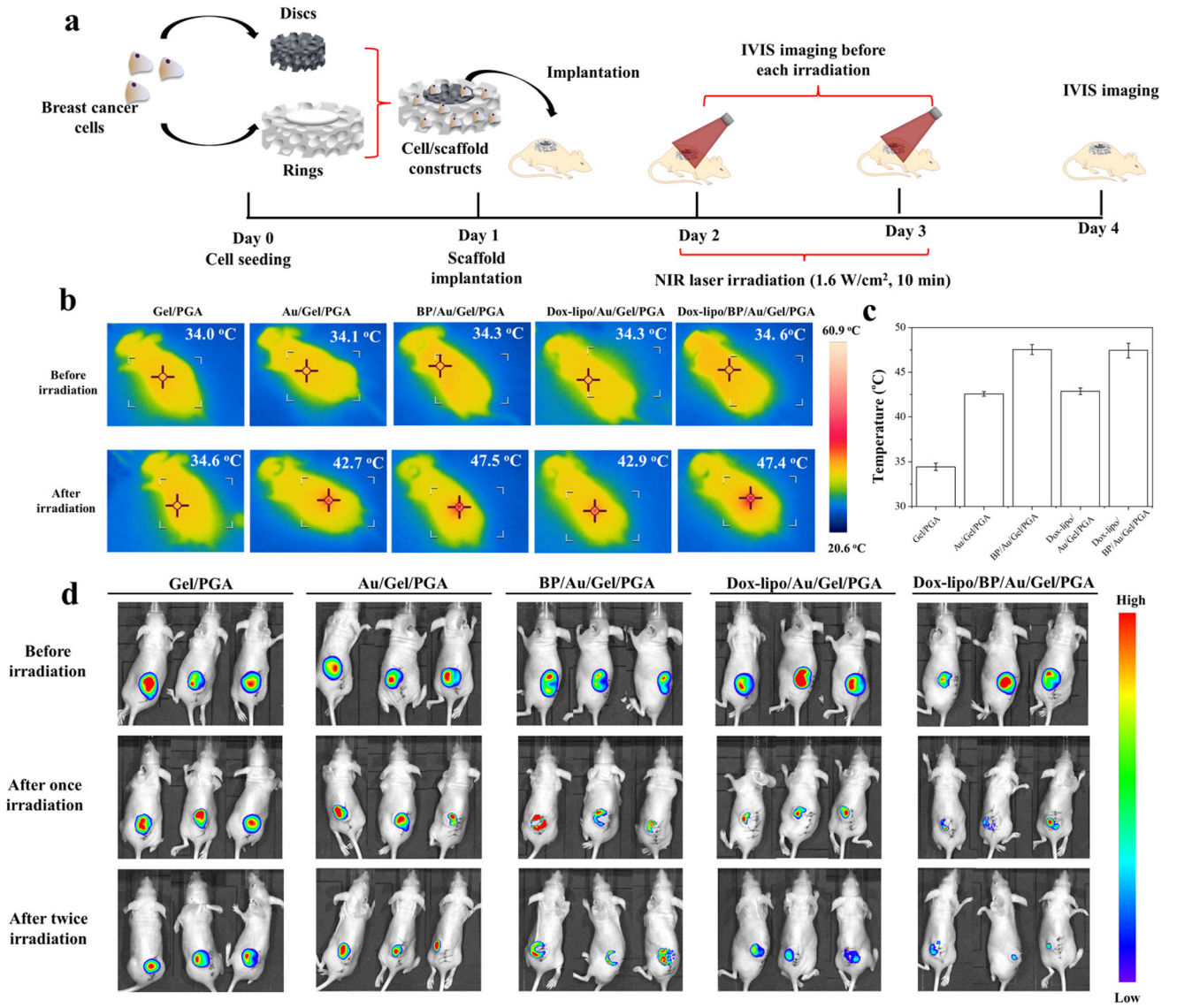


**Fig. 6** *In vivo* therapeutic effects of composite scaffolds after implantation. (a) Diagram of the animal experimental procedure. (b) IR thermographic images of mice subcutaneously implanted with different cell/scaffold constructs before and after NIR laser irradiation at an intensity of 1.6 W $cm^{-2}$ for 10 min after 1 d of implantation. (c) Temperature of different cell/scaffold constructs implanted in mice under NIR laser irradiation at an intensity of 1.6 W $cm^{-2}$ for 10 min after 1 d of implantation. Data are presented as the means ± S.D ($n$ = 3). (d) Whole-body bioluminescence images of mice subcutaneously implanted with breast cancer cell/scaffold constructs of the Gel/PGA, Au/Gel/PGA, BP/Au/Gel/PGA, Dox-lipo/Au/Gel/PGA and Dox-lipo/BP/Au/Gel/PGA composite scaffolds before and after laser irradiation (once and twice). Round discs of the cell/scaffold constructs were inserted into the central hole of the cell-seeded Gel/PGA scaffold rings and then subcutaneously implanted.

irradiation, the temperature of the irradiated region was monitored (Fig. 6b). The mice implanted with Gel/PGA composite scaffolds did not show local temperature change during laser irradiation. In contrast, after laser irradiation, the local temperatures of the mice implanted with the Au/Gel/PGA and Dox-lipo/Au/Gel/PGA composite scaffolds increased to 42.7 and 42.9 °C, respectively. The local temperatures of mice implanted with the BP/Au/Gel/PGA and Dox-lipo/BP/Au/Gel/PGA composite scaffolds increased to 47.5 and 47.4 °C, respectively (Fig. 6b and c). The temperature of the mouse skin region implanted with cell/scaffold constructs was lower than that measured in the PBS buffer (Fig. 3). This should be due to the influence of mouse skin on laser irradiation. The local temperatures of mice implanted with the Dox-lipo/Au/Gel/PGA and Dox-lipo/BP/Au/Gel/PGA composite scaffolds after laser irradiation were still higher than the liposome phase transition temperature. These results suggested that laser irradiation could facilitate the release of Dox from these two Dox-loaded composite scaffolds. Interestingly, the regional skin temperature of the mice implanted with Dox-lipo/Au/Gel/PGA after laser irradiation was near 42.9 °C, which was a mild hyperthermia environment and could reflect the condition of the Dox-lipo/BP/Au/Gel/PGA composite scaffolds after BP degradation. These results suggested that the Dox-lipo/BP/Au/Gel/PGA composite scaffolds after BP degradation could still generate a mild hyperthermia environment for the release of Dox.

The anticancer effects of the composite scaffolds were evaluated by IVIS imaging (Fig. 6d). All mice were irradiated with an NIR laser (1.6 W $cm^{-2}$, 10 min) twice. IVIS imaging was conducted before laser irradiation, 1 d after the first laser irradiation and 1 d after the second laser irradiation.

The IVIS images showed that all mice had strong bioluminescence signals at implant sites before laser irradiation, which suggested that the breast cancer cells cultured in the composite scaffolds were alive after implantation. The IVIS signals of the mice implanted with the Gel/PGA composite scaffolds were still strong after laser irradiation, which indicated that the Gel/PGA composite scaffolds had no anticancer effects. The mice implanted with the Au/Gel/PGA composite scaffolds showed slightly decreased bioluminescence signals after two laser irradiation cycles, which suggested that the mild hyperthermia environment had a limited effect on breast cancer cells. In contrast, the BP/Au/Gel/PGA composite scaffolds showed in an evident decrease in bioluminescence. The bioluminescence signal disappeared in the central region but remained in the scaffold ring region. The results indicated that the cells in the BP/Au/Gel/PGA composite scaffolds were ablated by NIR laser irradiation, while the breast cancer cells in the surrounding scaffold rings were not killed by the hyperthermia generated in the central composite scaffold discs. The bioluminescence signals of the mice implanted with the Dox-lipo/Au/Gel/PGA composite scaffolds were weaker than those of the mice implanted with the Au/Gel/PGA composite scaffolds. The accelerated release of Dox under NIR laser irradiation should work synergistically with mild hyperthermia to kill breast cancer cells more efficiently. The mice implanted with the Dox-lipo/BP/Au/Gel/PGA composite scaffolds showed the weakest bioluminescence signals after NIR laser irradiation. Most of the breast cancer cells in the central scaffold discs and in the surrounding scaffold rings were killed. Strong hyperthermia and accelerated Dox release should result in the most effective synergistic killing effect of the Dox-lipo/BP/Au/Gel/PGA composite scaffolds.

The long-term therapeutic effect of the Dox-lipo/BP/Au/Gel/PGA composite scaffolds was further investigated during implantation for 17 d (Fig. 7). Fig. 7a shows the time frame of cell seeding, culture, implantation, laser irradiation and IVIS imaging. The breast cancer cells were seeded in the Dox-lipo/BP/Au/Gel/PGA composite scaffold discs and Gel/PGA scaffold rings, assembled and implanted in the same way as the *in vivo* experiments shown in Fig. 6. However, the implants were not irradiated with an NIR laser until they completed 13 d of implantation, which allowed the degradation of the BPNSs in the composite scaffold discs. During the implantation without NIR laser irradiation, the local temperature of the implants was lower than the liposome phase transition temperature. Only a small amount of Dox should be released, as shown in Fig. 4a and a large amount of Dox should remain in the composite scaffolds. After 13 d of implantation, the implants were irradiated with NIR laser and the temperature of the irradiated region increased to 43.1 °C, which was lower than the temperature of the irradiated region when it was irradiated immediately after implantation (47.4 °C) (Fig. 7b and c). This should be due to the degradation of BPNSs and the photothermal convention effect of the remaining AuNRs. The AuNRs remaining in the composite scaffolds generated mild hyperthermia for the release of the remaining Dox. IVIS imaging showed that strong bioluminescence signals were detected immediately after implantation (Fig. 7d). After implantation for 13 d, the bioluminescence signals remained even though they were weakened, which could be attributed to the therapeutic effect of the slow release of Dox from the implanted Dox-lipo/BP/Au/Gel/PGA composite scaffolds. After each laser irradiation, the bioluminescence signals decreased due to mild hyperthermia and the accelerated release of Dox. After four times NIR laser irradiation, no bioluminescence was detected. The results indicated that mild hyperthermia and the accelerated release of Dox killed all the cells in the scaffold discs and scaffold rings (Fig. 7d).

The results of the *in vivo* anticancer effects of the composite scaffolds can be summarized as follows: first, the Au/Gel/PGA, Dox-lipo/Au/Gel/PGA and long-period implanted Dox-lipo/BP/Au/Gel/PGA composite scaffolds showed mild hyperthermia under NIR laser irradiation; second, the BP/Au/Gel/PGA and Dox-lipo/BP/Au/Gel/PGA composite scaffolds showed strong hyperthermia after short-period implantation; third, the Dox-lipo/Au/Gel/PGA and Dox-lipo/BP/Au/Gel/PGA composite scaffolds showed the synergistic effect of PTT and chemotherapy; and fourth, the Dox-lipo/BP/Au/Gel/PGA composite scaffolds showed the synergistic effect of strong PTT and chemotherapy immediately after implantation (early stage) and the chemotherapy effect of Dox after 13 d of implantation (late stage).

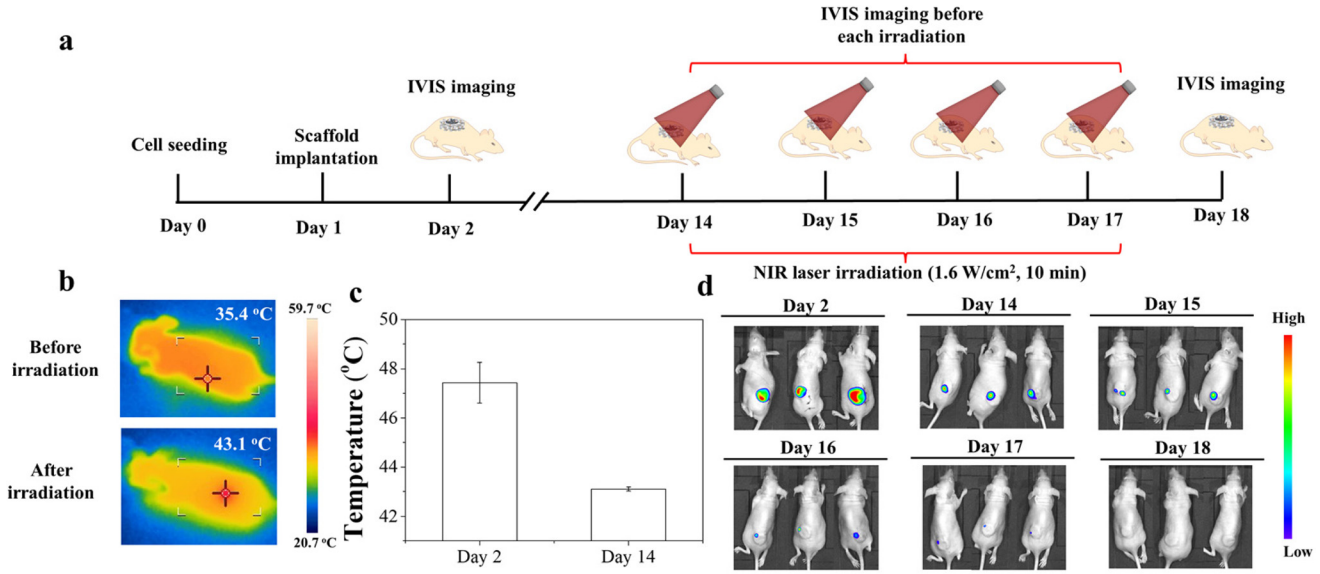


Fig. 7 Long-term *in vivo* therapeutic effect of Dox-lipo/BP/Au/Gel/PGA composite scaffolds. (a) Diagram of the animal experimental procedure. (b) IR thermographic images after 13 d of implantation and (c) local temperature of mice subcutaneously implanted with the breast cancer cell-seeded composite scaffolds before and after NIR laser irradiation at an intensity of 1.6 W $cm^{-2}$ for 10 min after 1 or 13 d of implantation. Data are the means ± S.D ($n$ = 3). (d) Whole-body bioluminescence images of mice subcutaneously implanted with breast cancer cell-seeded composite scaffolds after 1, 13, 14, 15, 16 and 17 d of implantation. Round discs of the cell/scaffold constructs were inserted into the central hole of the cell-seeded Gel/PGA scaffold rings and then subcutaneously implanted.

### Influence of composite scaffolds on hMSCs after the release of Dox

In addition to being used for their anticancer effects, the Dox-lipo/BP/Au/Gel/PGA composite scaffolds after Dox release could be used to promote the proliferation of stem cells to guide new tissue regeneration after killing the cancer cells because the main component of the composite scaffolds, gelatin, has peptides such as RGD for cell adhesion and proliferation. Therefore, the proliferation of hMSCs in the composite scaffolds after Dox release was evaluated. The Dox-lipo/BP/Au/Gel/PGA composite scaffolds were irradiated by an NIR laser 10 times to entirely release the Dox. Then, the hMSCs were cultured in the composite scaffolds for 3, 5 and 7 d. Live/dead staining showed that no dead cells were observed in the composite scaffolds after culturing for 3 d (Fig. 8a). The DNA quantification showed an increasing trend of amount of DNA (Fig. 8b). These results indicated that the composite scaffolds after complete release of Dox could support hMSC viability and proliferation.

PTT and chemotherapy have been combined for synergistic therapeutic outcomes.[4,41] However, a high temperature of PTT is not required for the chemotherapy effect, and a high temperature can cause unexpected damage to normal tissue.[42] In this study, a stepwise high-temperature PTT and mild-temperature chemotherapy was realized by incorporating stable AuNRs and degradable BPNSs in Dox-encapsulated thermosensitive liposome incorporated composite scaffolds. The Dox-lipo/BP/Au/Gel/PGA composite scaffolds showed high photothermal property due to the high photothermal conversion effects of the BPNSs and AuNRs.[34,43] After the degradation of BPNSs, the composite scaffolds showed a mild hyperthermic effect under NIR laser irradiation.

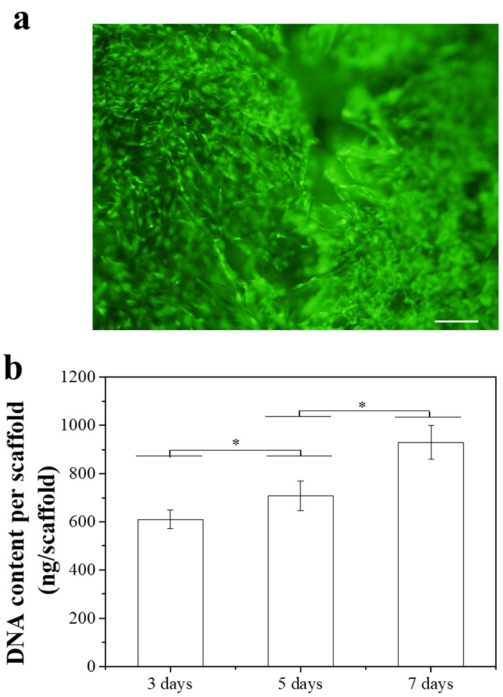


Fig. 8 Proliferation of hMSCs cultured in the Dox-lipo/BP/Au/Gel/PGA composite scaffolds after complete Dox release. (a) Live/dead staining of hMSCs after 3 d of culture. Scale bar: 200 μm. (b) Quantification of the DNA content of hMSC/scaffold constructs after culture for 3, 5 and 7 d. Data are the means ± S.D ($n$ = 3). Significant difference: *$p$ < 0.05.

The *in vitro* and *in vivo* experimental results indicated that the Dox-lipo/BP/Au/Gel/PGA composite scaffolds combined the effects of high-temperature PTT, which could ablate the breast cancer cells in the scaffolds, and mild hyperthermia, which could induce the accelerated release of Dox to kill the breast cancers that were outside the scaffolds. The composite scaffolds could kill breast cancer cells by the synergistic therapeutic effects of strong photothermal ablation and chemotherapy in the early stage of implantation and the synergistic therapeutic effects of mild hyperthermia and chemotherapy in the late stage of implantation. Moreover, the composite scaffolds after the release of Dox could support the proliferation of hMSCs, which might serve as supporting scaffolds to guide new tissue regeneration to recover tissue functions after killing the cancer cells. The composite scaffolds should be a potential smart platform for breast cancer therapy.

## Conclusion

AuNRs and degradable BPNSs were hybridized with Dox-encapsulated thermosensitive liposomes, PGA and gelatin to prepare Dox-lipo/BP/Au/Gel/PGA composite scaffolds for stepwise PTT and chemotherapy. The composite scaffolds had high photothermal conversion effects before BPNS degradation and mild hyperthermic effects after BPNS degradation. NIR laser irradiation triggered the accelerated release of Dox from the composite scaffolds. The Dox-lipo/BP/Au/Gel/PGA composite scaffolds could kill breast cancer cells by a synergistic effect of PTT and chemotherapy in the early stage and a chemotherapy effect in the late stage. A stepwise PTT and chemotherapy strategy was achieved by the composite scaffolds to effectively kill breast cancer cells inside the scaffolds or outside the scaffolds. Furthermore, the Dox-lipo/BP/Au/Gel/PGA composite scaffolds could support the proliferation of hMSCs for guiding new tissue regeneration after complete drug release. The composite scaffolds should be a smarter strategy for synergistic PTT and chemotherapy to treat breast cancer cells by overcoming the limitations of the current PTT and provide a better therapy strategy.

## Author contributions

H. C. contributed to the conceptualization, formal analysis, investigation, methodology, visualization, validation, data curation, and writing the original draft, revision and editing; R. S. contributed to the formal analysis and investigation; T. Z. contributed to the formal analysis and investigation; J. Z. contributed to the formal analysis and investigation; T. Y. contributed to the methodology and data curation; N. K. contributed to the funding acquisition, project administration, methodology, data curation, revision and editing; Y. Y. contributed to the methodology and data curation; G. C. contributed to the conceptualization, formal analysis, funding acquisition, project administration, investigation, methodology, resources, validation, data curation, supervision, and writing the original draft, revision and editing.

## Conflicts of interest

There are no conflicts to declare.

## Acknowledgements

This research was supported by JSPS KAKENHI Grant Number 19H04475 and 21H03830.

All animal procedures were performed in accordance with the Guidelines for Care and Use of Laboratory Animals of the National Institute for Materials Science and approved by the Animal Ethics Committee of the National Institute for Materials Science.

## References

1 J. Zhang, L. Yang, F. Huang, C. Zhao, J. Liu, Y. Zhang and J. Liu, *Adv. Healthcare Mater.*, 2021, **10**(21), e2101190.
2 X. Yang, L. Gao, Q. Guo, Y. Li, Y. Ma, J. Yang, C. Gong and C. Yi, *Nano Res.*, 2022, **13**, 2579–2594.
3 J. You, R. Zhang, G. Zhang, M. Zhong, Y. Liu, C. S. Van Pelt, D. Liang, W. Wei, A.K. Sood and C. Li, *J. Controlled Release*, 2012, **158**(2), 319–328.
4 V. D. Nguyen, H. K. Min, C. S. Kim, J. Han, J. O. Park and E. Choi, *Colloids Surf., B*, 2019, **173**, 539–548.
5 D. Zhi, T. Yang, J. O'Hagan, S. Zhang and R.F. Donnelly, *J. Controlled Release*, 2020, **325**, 52–71.
6 L. Zou, H. Wang, B. He, L. Zeng, T. Tan, H. Cao, X. He, Z. Zhang, S. Guo and Y. Li, *Theranostics*, 2016, **6**(6), 762–772.
7 S. Liu, X. Pan and H. Liu, *Angew. Chem., Int. Ed.*, 2020, **59**(15), 5890–5900.
8 A. L. Demain and P. Vaishnav, *Microb. Biotechnol.*, 2011, **4**(6), 687–699.
9 L. Cheng, X. Zhang, J. Tang, Q. Lv and J. Liu, *Biomaterials*, 2021, **275**, 120964.
10 S. Zhang, H. Chen, G. Zhang, X. Kong, S. Yin, B. Li and L. Wu, *J. Mater. Chem. B*, 2018, (2), 241–248.
11 Y. Yu, Y. Cheng, J. Tong, L. Zhang, Y. Wei and M. Tian, *J. Mater. Chem. B*, 2021, (13), 2979–2992.
12 F. Yan, W. Duan, Y. Li, H. Wu, Y. Zhou, M. Pan, H. Liu, X. Liu and H. Zheng, *Theranostics*, 2016, (13), 2337–2351.
13 L. Cheng, X. Zhang, J. Tang, Q. Lv and J. Liu, *Biomaterials*, 2021, **75**, 120964.
14 T. Tagami, M. J. Ernsting and S. D. Li, *J. Controlled Release*, 2011, **52**(2), 303–309.
15 H. Bi, J. Xue, H. Jiang, S. Gao, D. Yang, Y. Fang and K. Shi, *Asian J. Pharm. Sci.*, 2019, **14**(4), 365–379.
16 K. Kono, *Adv. Drug Delivery Rev.*, 2001, **53**(3), 307–319.

17 A. Refaat, B. Del Rosal, J. Palasubramaniam, G. Pietersz, X. Wang, S. E. Moulton and K. Peter, *J. Controlled Release*, 2021, **337**, 212–223.
18 J. Shi, P. W. Kantoff, R. Wooster and O. C. Farokhzad, *Nat. Rev. Cancer*, 2017, **17**(1), 20–37.
19 C. Wong, T. Stylianopoulos, J. Cui, J. Martin, V. P. Chauhan, W. Jiang, Z. Popovic, R. K. Jain, M. G. Bawendi and D. Fukumura, *Proc. Natl. Acad. Sci. U. S. A.*, 2011, **108**(6), 2426–2431.
20 J. Zhang, J. Li, N. Kawazoe and G. Chen, *J. Mater. Chem. B*, 2017, **5**(2), 245–253.
21 Q. Yu, Y. Han, X. Wang, C. Qin, D. Zhai, Z. Yi, J. Chang, Y. Xiao and C. Wu, *ACS Nano*, 2018, **2**(3), 2695–2707.
22 Y. Liu, T. Li, H. Ma, D. Zhai, C. Deng, J. Wang, S. Zhuo, J. Chang and C. Wu, *Acta Biomater.*, 2018, **3**, 531–546.
23 L. Ma, Y. Zhou, Z. Zhang, Y. Liu, D. Zhai, H. Zhuang, Q. Li, J. Yue, C. Wu and J. Chang, *Sci. Adv.*, 2020, (32), eabb1311.
24 X. Wang, B. Ma, J. Xue, J. Wu, J. Chang and C. Wu, *Nano Lett.*, 2019, **9**(3), 2138–2147.
25 X. Wang, F. Lv, T. Li, Y. Han, Z. Yi, M. Liu, J. Chang and C. Wu, *ACS Nano*, 2017, **1**(11), 11337–11349.
26 H. Ma, Q. Zhou, J. Chang and C. Wu, *ACS Nano*, 2019, **3**(4), 4302–4311.
27 X. Wang, J. Zhang, J. Li, Y. Chen, Y. Chen, N. Kawazoe and G. Chen, *J. Mater. Chem. B*, 2018, **6**(46), 7728–7736.
28 R. Xing, K. Liu, T. Jiao, N. Zhang, K. Ma, R. Zhang, Q. Zou, G. Ma and X. Yan, *Adv. Mater.*, 2016, **28**(19), 3669–3676.
29 H. Chen, R. Sun, J. Zheng, N. Kawazoe, Y. Yang and G. Chen, *J. Mater. Chem. B*, 2022, **10**(25), 4771–4782.
30 A. López-Noriega, E. Ruiz-Hernández, E. Quinlan, G. Storm, W. E. Hennink and F. J. O'Brien, *J. Controlled Release*, 2014, **187**, 158–166.
31 L. Sutrisno, H. Chen, T. Yoshitomi, N. Kawazoe, Y. Yang and G. Chen, *J. Mater. Chem. B*, 2022, **10**(2), 204–213.
32 H. Chen, X. Wang, L. Sutrisno, T. Zeng, N. Kawazoe, Y. Yang and G. Chen, *Front. Bioeng. Biotechnol.*, 2020, **8**, 589905.
33 H. Liu, Y. Mei, Q. Zhao, A. Zhang, L. Tang, H. Gao and W. Wang, *Pharmaceutics*, 2021, **13**(9), 1344.
34 J. Shao, H. Xie, H. Huang, Z. Li, Z. Sun, Y. Xu, Q. Xiao, X. F. Yu, Y. Zhao, H. Zhang, H. Wang and P. K. Chu, *Nat. Commun.*, 2016, **7**, 12967.
35 W. Chen, J. Ouyang, H. Liu, M. Chen, K. Zeng, J. Sheng, Z. Liu, Y. Han, L. Wang, J. Li, L. Deng, Y. Liu and S. Guo, *Adv. Mater.*, 2017, **29**, 1603864.
36 M. F. Tsai, S. H. Chang, F. Y. Cheng, V. Shanmugam, Y. S. Cheng, C. H. Su and C. S. Yeh, *ACS Nano*, 2013, **7**(6), 5330–5342.
37 Y. Wang, K. C. Black, H. Luehmann, W. Li, Y. Zhang, X. Cai, D. Wan, S. Y. Liu, M. Li, P. Kim, Z. Y. Li, L. V. Wang, Y. Liu and Y. Xia, *ACS Nano*, 2013, **7**(3), 2068–2077.
38 L. Sutrisno, H. Chen, Y. Chen, T. Yoshitomi, N. Kawazoe, Y. Yang and G. Chen, *Biomaterials*, 2021, **275**, 120923.
39 M. Qiu, D. Wang, W. Liang, L. Liu, Y. Zhang, X. Chen, D. K. Sang, C. Xing, Z. Li, B. Dong, F. Xing, D. Fan, S. Bao, H. Zhang and Y. Cao, *Proc. Natl. Acad. Sci. U. S. A.*, 2018, **115**(3), 501–506.
40 J. Li, J. Wang, J. Zhang, T. Han, X. Hu, M. M. S. Lee, D. Wang and B. Tang, *Adv. Mater.*, 2021, **33**(51), e2105999.
41 Y. Su, Z. Teng, H. Yao, S. Wang, Y. Tian, Y. Zhang, W. Liu, W. Tian, L. Zheng, N. Lu, Q. Ni, X. Su, Y. Tang, J. Sun, Y. Liu, J. Wu, G. Yang, G. Lu and L. Zhang, *ACS Appl. Mater. Interfaces*, 2016, **8**(27), 17038–17046.
42 H. Cai, X. Dai, X. Guo, L. Zhang, K. Cao, F. Yan, B. Ji and Y. Liu, *Acta Biomater.*, 2021, **127**, 276–286.
43 X. Wang, J. Li, N. Kawazoe and G. Chen, *Materials*, 2018, **12**(1), 31.

 